Taylor & Francis
Taylor & Francis Group

Check for updates

# A boundary element implementation for fracture mechanics problems using generalised Westergaard stress functions

Ney Augusto Dumont [a], Elvis Yuri Mamani [b]
and Marilene Lobato Cardoso [a]

[a]Department of Civil and Environmental Engineering, PUC-Rio – Pontifical Catholic University of Rio de Janeiro, Rio de Janeiro, Brazil; [b]Universidad Andina del Cusco, Urbanización Ingeniería, Cusco, Perú

**ABSTRACT**

In the traditional boundary element methods, the numerical modelling of cracks is usually carried out by means of a hypersingular fundamental solution, which involves a $1/r^2$ kernel for two-dimensional problems. A more natural procedure should make use of fundamental solutions that represent the square root singularity of the gradient field around the crack tip (a Green's function). Such a representation has been already accomplished in a variationally based framework that also addresses a convenient means of evaluating results at internal points. This paper proposes a procedure for the numerical simulation of two-dimensional problems with a fundamental solution that can be in part or for the whole structure based on generalised Westergaard stress functions. Problems of general topology can be modelled, such as in the case of unbounded and multiply-connected domains. The formulation is naturally applicable to notches and generally curved cracks. It also provides an easy means of evaluating stress intensity factors, when particularly applied to fracture mechanics. The main features of the theory are briefly presented in the paper, together with several validating examples and some convergence assessments.

## 1. Previous developments and motivation

### 1.1. Introduction

Irwin (1957), Sneddon (1946), Westergaard (1939) and Williams (1957) are some of the very first researchers to investigate the isotropic linear elastic material behaviour ahead of a crack tip (see also Anderson, 1995). Since then, a considerable effort has been done in the engineering community to understand and model the phenomenon. Some of these contributions may be worth mentioning: Ang and Telles (2004); Barenblatt (1962); Brown and

Strawley (1966); Dugdale (1960); Eftis and Liebowitz (1972); Harmain and Provan (1997); Jing, Khraishi, and Gorbatikh (2003); Sousa, Castro, Lopes, and Martha (2013); Telles, Castor, and Guimares (1995); Xin, Hangong, Xingwu, and Liangzhou (2010); and Zhang, Qiang, and Yang (2007). The most accurate models rely on finite element simulations that require as a rule very fine domain meshes, are time consuming and demand from the analyst great discernment to adequately retrieve results.

Tada, Ernst, and Paris (1993, 1994) proposed a simple method for the construction of Westergaard-type stress functions for the analysis of fracture mechanics problems with either prescribed displacements or stresses. Their developments were restricted to the mathematical aspects of the formulation and to some analytical unfoldings. The concept proposed by these authors is now generalised and used for the construction of fundamental solutions in the hybrid boundary element method (HBEM), which can be advantageously applied to classical elasticity problems and specifically to fracture mechanics (Dumont & Lopes, 2003; Dumont & Mamani, 2011a; b, 2013). This formulation is directly applicable to notches as well as to internal or external curved cracks and enables the adequate description of high stress gradients: it is thus a simple means of evaluating stress intensity factors. Moreover, it is possible to use such stress functions to obtain the plastic zone around a crack tip in the frame of an iterative procedure (Dumont & Mamani, 2013). This paper is a further generalisation of the developments proposed by Dumont and Mamani (2011b) towards the implementation of more accurate stress functions, as also illustrated with a few basic, academical examples.

## 1.2. *Previous developments*

A superposition of cracks was proposed by Dumont and Lopes (2003) to simulate cracks of general shape, as given on the top of Figure 1. The illustrated five nodal parameters are related to tractions given by Westergaard complex stress functions, applied as a succession of straight crack elements along the curved crack. An improvement of these developments could be obtained later on by Dumont and Mamani (2011a, 2011b) in terms of superposed semicracks, as outlined in Section 3 and illustrated on the bottom of Figure 1, not only to better fit curved cracks but also to simulate cavities, corners and notches. Based on these developments, Dumont and Mamani (2013) also proposed the use of the model for the simulation of small plastic zones that develop and propagate around cracks.
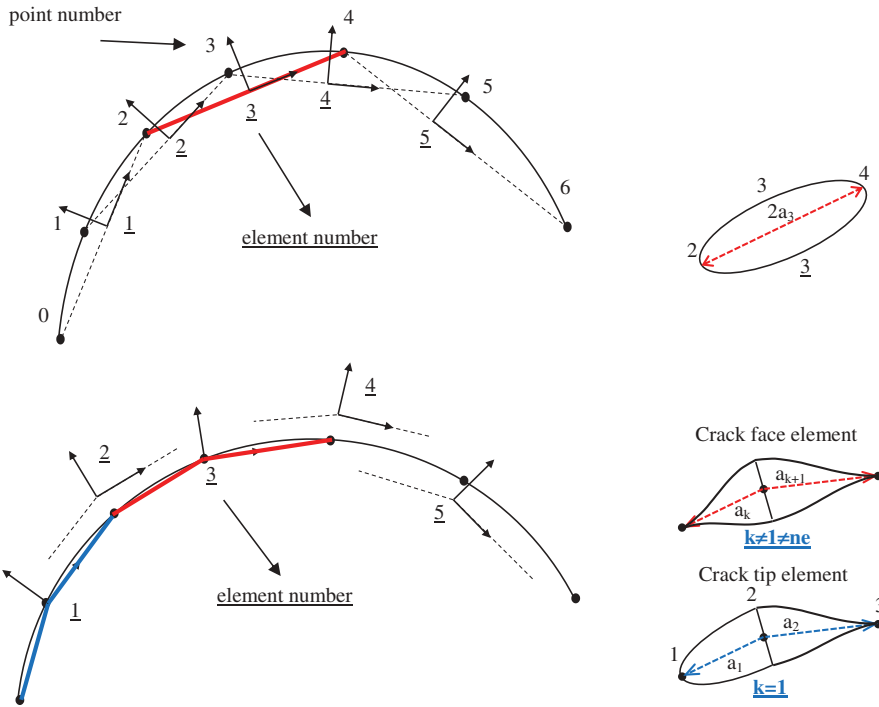
**Figure 1.** Illustration of the use of straight cracks to simulate generally curved cracks, on the top (Dumont & Lopes, 2003), now improved with the use of kinked cracks of different shapes (Mamani, 2015), on the bottom.

### 1.3. *Motivation*

The primary motivation of the present theoretical developments is a better simulation of the stress field around crack tips that may lead to accurate stress intensity factors as well as to the adequate representation of plastic zones. The elliptic semicrack proposed by Dumont & Mamani (2011a, b, 2013), which seems efficient for the description of the stress field around crack tips, should be combined with crack elements of different shapes, so that spurious stress singularities in regions along the crack face can be avoided or minimised.

The present proposition consists in the use of semielliptic cracks to represent crack tips only, with (Hermite) polynomial-shaped openings for the simulation of the remaining of the crack face, as shown on the bottom of Figure 1. It is a sequel of the works done by the first author with his former students Lopes and Mamani and incorporates some unpublished results by Mamani (2015) as well as from an MSc research that has just been finished (Cardoso, 2017). It also uses and expands materials from two previous conference articles (Dumont, Mamani, & Cardoso, 2017; Mamani & Dumont, 2015). As developed in Section 5, this is still a work in progress as the general combination of all features described in this paper and

mainly by Dumont and Mamani (2011b) demands a high degree of mathematical understanding and unfoldings before it can be considered accomplished.

## 2. Brief outline of the HBEM

The HBEM was introduced in 1987 on the basis of the Hellinger–Reissner potential and as a generalisation of Pian's hybrid finite element method (Dumont, 1989; Pian, 1964). The formulation requires evaluation of integrals only along the boundary and makes use of fundamental solutions (Green's functions) to interpolate fields in the domain. Accordingly, an elastic body of arbitrary shape may be treated as a single finite macro-element with as many boundary degrees of freedom as desired. In the meantime, the formulation has evolved to several application possibilities, including time-dependent problems (Dumont & De Oliveira, 2001), fracture mechanics (Dumont & Lopes, 2003), non-homogeneous materials (Dumont, Chaves, & Paulino, 2004) and strain gradient elasticity (Dumont & Huaman, 2009).

The brief outline of Sections 2.1–2.3 is presented according to Dumont and Mamani (2011b).

### 2.1. Problem formulation

An elastic body is submitted to body forces $b_i$ in the domain, tractions $\bar{t}_i$ on part $\Gamma_\sigma$ of the boundary $\Gamma$ and to displacements $\bar{u}_i$ on the complementary part $\Gamma_u$ . The task is to find the best approximation for stresses and displacements, $\sigma_{ij}$ and $u_i$, such that

$$\sigma_{ji,j} = b_i \quad \text{in the domain} \quad \Omega, \tag{1}$$

$$u_i = \bar{u}_i \quad \text{along} \quad \Gamma_u, \tag{2}$$

$$t_i = \sigma_{ij} n_j = \bar{t}_i \quad \text{along} \quad \Gamma_\sigma \tag{3}$$

in which $n_j$ is the outward unit normal to the boundary. Indicial notation is used.

### 2.2. Stress and displacement assumptions

Two independent trial fields are assumed (Dumont, 1989; Pian, 1964). The displacement field is explicitly approximated along the boundary by $u_i^d$, where $()^d$ means *displacement assumption*, in terms of polynomial functions $u_{im}$ with compact support and nodal displacement

parameters $\mathbf{d} = [d_m] \in R^{n^d}$, for $n^d$ displacement degrees of freedom of the discretised model. An independent stress field $\sigma_{ij}^s$, where $()^s$ stands for *stress assumption*, is given in the domain in terms of a series of fundamental solutions $\sigma_{ijm}^*$ with global support, multiplied by force parameters $\mathbf{p}^* = [p_m^*] \in R^{n^*}$ applied at the same boundary nodal points $m$ to which the nodal displacements $d_m$ are attached ($n^* = n^d$), plus some particular solution $\sigma_{ij}^p$ due to body forces, for instance. Displacements $u_i^s$ are obtained from $\sigma_{ij}^s$. Then,

$$u_i^d = u_{im} d_m \quad \text{on} \quad \Gamma \quad \text{such that} \quad u_i^d = \bar{u}_i \quad \text{on} \quad \Gamma_u \quad \text{and} \tag{4}$$

$$\sigma_{ij}^s = \sigma_{ijm}^* p_m^* + \sigma_{ij}^p \quad \text{such that} \quad \sigma_{jim,j}^* = 0 \quad \text{in} \quad \Omega \tag{5}$$

$$\Rightarrow \quad u_i^s = u_{im}^* p_m^* + u_{is}^r C_{sm} p_m^* + u_i^p \quad \text{in} \quad \Omega \tag{6}$$

where $u_{im}^*$ are displacement fundamental solutions corresponding to $\sigma_{ijm}^*$. Rigid body motion is included in terms of functions $u_{is}^r$ multiplied by in principle arbitrary constants $C_{sm}$ (Dumont, 1989).

## 2.3. Governing matrix equations

The Hellinger–Reissner potential, as implemented by Pian (1964) on the basis of the two-field assumptions of the latter section and generalised by Dumont (1989), leads to two matrix equations that express nodal equilibrium and compatibility requirements:

$$\mathbf{H}^{\mathrm{T}} \mathbf{p}^* = \mathbf{p} - \mathbf{p}^p \tag{7}$$

$$\mathbf{F}^* \mathbf{p}^* = \mathbf{H}(\mathbf{d} - \mathbf{d}^p) \tag{8}$$

in which $\mathbf{H} = [H_{nm}] \in R^{n^d \times n^*}$ is the same double-layer potential matrix of the collocation boundary element method (Brebbia, Telles, & Wrobel, 1984) and $\mathbf{F}^* = [F_{nm}^*] \in R^{n^* \times n^*}$ is a symmetric, flexibility matrix. The force and displacement parameters $\mathbf{p}^\star$ and $\mathbf{d}$, introduced in the previous section, are the problem's primary unknowns. Moreover, $\mathbf{p} = [p_n] \in R^{n^d}$ and $\mathbf{p}^p = [p_n^p] \in R^{n^d}$ are nodal forces equivalent to applied boundary tractions and body forces, respectively, and $\mathbf{d}^p = [d_n^p] \in R^{n^d}$ are nodal displacements corresponding to $\mathbf{p}^p$. The matrices $\mathbf{H}$ and $\mathbf{F}^*$ may be compactly defined as

$$\begin{bmatrix} H_{mn} & F_{mn}^* \end{bmatrix} = \int_\Gamma \sigma_{ijm}^* n_j \langle u_{in} \quad u_{in}^* \rangle \mathrm{d}\Gamma \tag{9}$$

Solving for $\mathbf{p}^*$ in Eq. (7), one arrives at the matrix system

$$\mathbf{H}^{\mathrm{T}}\mathbf{F}^{*(-1)}\mathbf{H}(\mathbf{d} - \mathbf{d}^p) = \mathbf{p} - \mathbf{p}^p \qquad (10)$$

where $\mathbf{H}^{\mathrm{T}}\mathbf{F}^{*(-1)}\mathbf{H} \equiv \mathbf{K}$ is a stiffness matrix. The inverse $\mathbf{F}^{*(-1)}$ must be evaluated in terms of generalised inverses as $\mathbf{F}^*$ is singular for a finite domain $\Omega$ (Dumont, 1989). Results at internal points are expressed in terms of Eqs. (5) and (6) after evaluation of $\mathbf{p}^*$ .

Since evaluating $\mathbf{F}$ and solving for $\mathbf{p}^*$ in Eq. (8) is very time consuming, a simplified hybrid boundary formulation has been developed (Dumont & Aguilar, 2012) to completely circumvent the matrix operations described in the latter paragraph. On the other hand, the present problem of fracture mechanics is usually formulated for Neumann-type boundary conditions, for which Eq. (7) is sufficient and then only the double-layer potential matrix $\mathbf{H}$ must be evaluated.

Although initially proposed in the frame of the HBEM, the present developments can be applied to the conventional, collocation boundary element method (Cardoso, 2017):

$$\mathbf{G}(\mathbf{t} - \mathbf{t}^p) = \mathbf{H}(\mathbf{d} - \mathbf{d}^p) \qquad (11)$$

with the single layer potential matrix $G_{m\ell} \equiv \mathbf{G}$ and the vectors of traction forces $t_\ell \equiv \mathbf{t}$ and $t_\ell^p \equiv \mathbf{t}^p$ that correspond to applied boundary and body forces, respectively (Dumont, 2014).

## 3. Stress functions

As proposed by Tada et al. (1993, 1994), fundamental solutions (Green's functions) may be obtained for a prescribed crack opening of shape $f(x)$ in the interval $[x_1, x_2]$ along the $x$ axis – and symmetric with respect to this axis in the Cartesian coordinate system $(x, y)$ – in terms of the potential function $\Phi(z)$

$$\Phi(z) = -\frac{1}{2\pi} \int_{x_1}^{x_2} \frac{f(x)}{z - x} \mathrm{d}x \qquad (12)$$

This procedure, which may be deemed a generalisation of the work done by Crouch and Starfield (1983), has been further generalised by Dumont and Mamani (2011b) for the composition of kinked cracks of any length, as illustrated in Figures 1 and 2. To make calculations as simple as possible, one defines the Green's function $\Phi(Z_1)$ for the shape function initially given for a semicrack (numbered as 1, indicated by the subscript) with length $a_1 = 1$ and the integration of Eq. (12) is carried out in the interval $[x_1, x_2] \equiv [0, 1]$ . The generalisation for a semicrack of length $a_1$ and rotated by an angle $\theta_1$ is given by
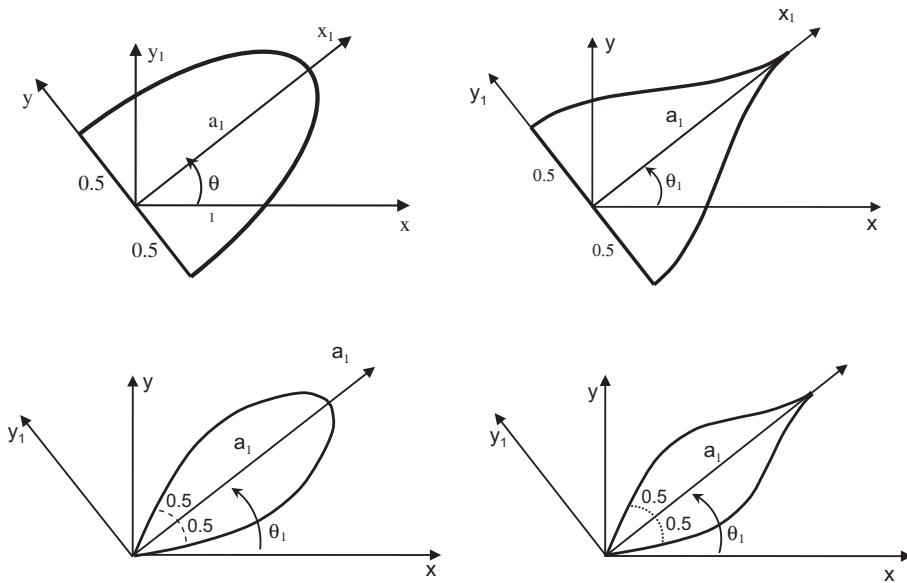
**Figure 2.** Semicracks of length $a_1$ rotated by an angle $\theta_1$ : elliptic and polynomial openings at $x = 0$ (top), relative crack face rotations at $x = 0$ (down) (Mamani & Dumont, 2015).

$$Z_1 = zT_1 \equiv \frac{z}{a_1}\mathrm{e}^{-i\theta_1} \equiv \frac{x + iy}{a_1}\mathrm{e}^{-i\theta_1} \equiv \frac{r}{a_1}\mathrm{e}^{i(\theta - \theta_1)} \tag{13}$$

The next section applies the procedure just outlined to show that the original proposition by Westergaard can be retrieved as a particular case. The generalisation for elliptic and polynomial semicrack openings – as well as for the introduction of the relative rotation of two adjacent crack faces – is proposed subsequently.

## 3.1. Consistent formulation of the original Westergaard stress function for an elliptic crack

The stress function $\Phi$ originally proposed by Westergaard may be obtained from Eq. (12), for the elliptic crack shape illustrated on top right of Figure 1. In fact, for a normalised semiwidth $a_1 = 1$, corresponding to the integration interval $[x_1, x_2] \equiv [-1, 1]$ and in terms of a local coordinate system such that $Z$ in Eq. (13) refers to an angle $\theta_1 = 0$, $\Phi$ in Eq. (12) is obtained as

$$f(x) = \sqrt{1 - x^2}, \quad -1 \leq x \leq 1, \Rightarrow \Phi = \frac{\sqrt{Z^2 - 1}}{2}\frac{\sqrt{Z^2}}{Z} - \frac{Z}{2} \tag{14}$$

The expression of $f(x)$ above is an ellipsis of length 2. The identity $\mathrm{csgn}(Z) \equiv \sqrt{Z^2}/Z$ in the expression of $\Phi$ is software-independent and

convenient to implement (Dumont & Lopes, 2003). Using polar coordinates centred at the crack tip ($Z = 1$), such that $Z = 1 + re^{\theta i}$, one obtains for the leading terms (terms that do not tend to zero as $r \to 0$) of the expressions of $\Phi$ and its derivatives given in Eq. (14):

$$\lim_{r \to 0} \Phi = \sqrt{\frac{r}{2}} e^{\theta i/2} \; ; \quad \lim_{r \to 0} \Phi' = \frac{1}{2\sqrt{2r}} e^{-\theta i/2} - \frac{1}{2} ; \quad \lim_{r \to 0} \Phi'' = \frac{-1}{4r\sqrt{2r}} e^{-3\theta i/2}$$

$$(15)$$

Observe in the above as well as in the following expressions that some constant terms automatically appear as $r \to 0$. These terms are not part of Westergaard's original expressions, which have been proposed for a remote biaxial stress field. In fact, the present and following formulations correspond to traction forces applied to a crack opening, thus leading to a stress field that vanishes at infinity. The present elliptic opening refers to unit, constant traction forces, but this configuration varies considerably depending on the prescribed crack opening, as shown in Figure 2. The constant terms in $\Phi'$ above and in the following developments correspond to 'T stresses' (which cause transversal contraction of the cracked specimen), as already reported in the literature (Gupta, Alderliesten, & Benedictus, 2015).

One should bear in mind that the 'leading terms' shown in the latter equations as well as in the following equations for the limit $r \to 0$ only contain the higher order terms and constants. As explained by Dumont and Mamani (2011b), the hypersingular kernel $r^{-3/2}$ in the expression of $\Phi''$ in Eq. (15) does not lead to any mathematical issues in the stress expressions along a crack face – as developed in Section 4 – since the corresponding terms cancel out when two cracks or semicracks are superposed independently from their relative orientation, as illustrated in Figure 1. This remark is also valid for similar hypersingularities that come out in the developments of the next section.

### 3.2. Generalised Westergaard stress functions for different types of semicrack openings in the local, normalised interval $[x_1, x_2] \equiv [0, 1]$

The expression of $\Phi$ in Eq. (12) for an elliptic semicrack opening at the crack tip – the top-left opening configuration of Figure 2 and in terms of the normalised, local coordinate system $[x_1, x_2] \equiv [0, 1]$ – is given by

$$f(x) = \sqrt{1 - x^2} \Rightarrow \Phi = \frac{\sqrt{1 - Z^2}}{2\pi} \ln\left(\frac{-1 - \sqrt{1 - Z^2}}{Z}\right) - \frac{2 + Z\pi}{4\pi} \quad (16)$$

Observe that $f(x), x \in [0, 1]$, is a semiellipsis such that $f(0) = 1, f'(0) = 0$ and $f(1) = 0, f'(1^-) \to -\infty$ .

For a polynomial semicrack opening – corresponding to the top-right configuration of Figure 2 – the expression of $\Phi$ in Eq. (12) is

$$f(x) = 2x^3 - 3x^2 + 1 \Rightarrow \Phi$$
$$= \frac{1 - 3Z^2 + 2Z^3}{2\pi} \ln\left(\frac{Z-1}{Z}\right) - \frac{5 + 12Z - 12Z^2}{12\pi} \tag{17}$$

The function $f(x), x \in [0, 1]$, above is a Hermitian polynomial, such that $f(0) = 1, f'(0) = 0$ and $f(1) = f'(1) = 0$ .

On the other hand, the expression of $\Phi$ in Eq. (12) for the relative face rotation of the semicrack that lies at the crack tip, as given on the bottom-left opening configuration of Figure 2:

$$f(x) = x\sqrt{1 - x^2} \Rightarrow \Phi$$
$$= \frac{Z\sqrt{1 - Z^2}}{2\pi} \ln\left(\frac{-1 - \sqrt{1 - Z^2}}{Z}\right) - \frac{-\pi + 4Z + 2\pi Z^2}{8\pi} \tag{18}$$

The function $f(x), x \in [0, 1]$, above is such that $f(0) = 0, f'(0) = 1$ and $f(1) = 0, f'(1^-) \to -\infty$ .

Finally, one obtains the expression of $\Phi$ in Eq. (12) for the relative face rotation of a semicrack along the crack face, as shown as the bottom-left opening configuration of Figure 2, as

$$f(x) = x^3 - 2x^2 + x \Rightarrow \Phi$$
$$= \frac{Z - 2Z^2 + Z^3}{2\pi} \ln\left(\frac{Z-1}{Z}\right) - \frac{1}{12\pi}\left(-2 + 9Z - 6Z^2\right) \tag{19}$$

The function $f(x), x \in [0, 1]$, above is also a Hermitian polynomial, such that $f(0) = 0, f'(0)1$ and $f(1) = f'(1) = 0$ .

The leading terms of all four generalised Westergaard functions $\Phi$ given above as well as of their derivatives both at the semicrack tip $Z = 1$ (writing $Z = 1 + re^{\theta i}$) and at internal interface $Z = 0$ (writing $Z = re^{\theta i}$) are given in Table 1.

In the series expansions necessary to arrive at the leading term results of Table 1, the transcendental parts are multiplied by $\lim_{r \to 0^+} \text{csgn}\left(i\left(1 + \sqrt{1 - (1 + re^{i\theta})^2}\right)/(1 + re^{i\theta})\right)$, whose evaluation may become tricky. However, one may just compare these equations with the corresponding terms in Eq. (15) and thus infer the correct sign to be assigned.

**Table 1.** Leading terms and constants of the functions $\Phi$ defined in Section 3.2 and their derivatives at either extremity of the defined semicracks.

| | Equation number | $\lim\limits_{r\to 0} \Phi$ | $\lim\limits_{r\to 0} \Phi'$ | $\lim\limits_{r\to 0} \Phi''$ |
|---|---|---|---|---|
| Limit for $Z = 1 + re^{\theta i}$ | (16) | $\sqrt{\frac{r}{2}}e^{\theta i/2} - \frac{2+\pi}{4\pi}$ | $\frac{e^{-\theta i/2}}{2\sqrt{2r}} - \frac{4+\pi}{4\pi}$ | $\frac{-e^{-3\theta i/2}}{4r\sqrt{2r}}$ |
| | (17) | $-\frac{5}{12\pi}$ | $\frac{1}{\pi}$ | $\frac{3\ln(re^{\theta i})}{\pi} + \frac{13}{2\pi}$ |
| | (18) | $\sqrt{\frac{r}{2}}e^{\theta i/2} - \frac{4+\pi}{8\pi}$ | $\frac{e^{-\theta i/2}}{2\sqrt{2r}} - \frac{3+\pi}{2\pi}$ | $\frac{-e^{-3\theta i/2}}{4r\sqrt{2r}}$ |
| | (19) | $-\frac{1}{12\pi}$ | $-\frac{1}{12\pi}$ | $\frac{\ln(re^{\theta i})}{\pi} + \frac{5}{2\pi}$ |
| Limit for $Z = re^{\theta i}$ | (16) | $\frac{1}{2\pi}\ln\left(\frac{2}{re^{\theta i}}\right) - \frac{i\pi+1}{2\pi}$ | $\frac{-e^{-\theta i}}{2\pi r} - \frac{1}{4}$ | $\frac{e^{-2\theta i}}{2\pi r^2} + \frac{i\pi+1}{2\pi}$ |
| | (17) | $\frac{1}{2\pi}\ln\left(\frac{-1}{e^{\theta i}r}\right) - \frac{5}{12\pi}$ | $\frac{-e^{-\theta i}}{2\pi r}$ | $\frac{e^{-2\theta i}}{2\pi r^2}$ |
| | (18) | $\frac{1}{8}$ | $\frac{1}{2\pi}\ln\left(\frac{-2}{e^{\theta i}r}\right) - \frac{1}{\pi}$ | $\frac{-e^{-\theta i}}{2\pi r}$ |
| | (19) | $\frac{1}{6\pi}$ | $\frac{1}{2\pi}\ln\left(\frac{-1}{e^{\theta i}r}\right) - \frac{5}{4\pi}$ | $\frac{-e^{-\theta i}}{2\pi r}$ |

## 4. The crack modelling problem

### 4.1 Basic developments

Independently from the proposed stress function, as shown in the previous section, the mode I and mode II crack opening displacement and stress expressions for plane strain are (Dumont & Mamani, 2011b; Mamani, 2011)

$$
\mathbf{u}^I_{(0)} = \frac{1+\nu}{E}\left\{ \begin{array}{c} (1-2\nu)\mathrm{Re}\Phi - \frac{y}{a}\mathrm{Im}\Phi' \\ 2(1-\nu)\mathrm{Im}\Phi - \frac{y}{a}\mathrm{Re}\Phi' \end{array} \right\}, \quad \sigma^I_{(0)} = \begin{bmatrix} \frac{1}{a}\mathrm{Re}\Phi' - \frac{y}{a^2}\mathrm{Im}\Phi'' \\ \frac{1}{a_1}\mathrm{Re}\Phi' + \frac{y}{a^2}\mathrm{Im}\Phi'' \\ -\frac{y}{a^2}\mathrm{Re}\Phi'' \end{bmatrix}
$$

(20)

$$
\mathbf{u}^{II}_{(0)} = \frac{1+\nu}{E}\left\{ \begin{array}{c} 2(1-\nu)\mathrm{Im}\Phi + \frac{y}{a}\mathrm{Re}\Phi' \\ -(1-2\nu)\mathrm{Re}\Phi - \frac{y}{a}\mathrm{Im}\Phi' \end{array} \right\}, \quad \sigma^{II}_{(0)} = \begin{bmatrix} \frac{2}{a}\mathrm{Im}\Phi' + \frac{y}{a^2}\mathrm{Re}\Phi'' \\ -\frac{y}{a^2}\mathrm{Re}\Phi'' \\ \frac{1}{a}\mathrm{Re}\Phi' - \frac{y}{a^2}\mathrm{Im}\Phi'' \end{bmatrix}
$$

(21)

The subscript $()_{(0)}$ in the above equations means that all quantities are referred to the semicrack's local Cartesian system, as $(x_1, y_1)$ in Figure 2, and must be consequently rotated to the global system, according to Eq. (13).

A general kinked crack is obtained by combining two semicracks, as shown schematically in Figure 3 for two elliptic semicracks. In this figure, mode $I$ and $II$ traction forces $(p_1^I, p_1^{II})$ and $(p_2^I, p_2^{II})$ are schematically represented along the interfaces of semicracs 1 and 2 . They are brought in dependence of nodal force parameters $p_x^\star$ and $p_y^\star$ in such a way that
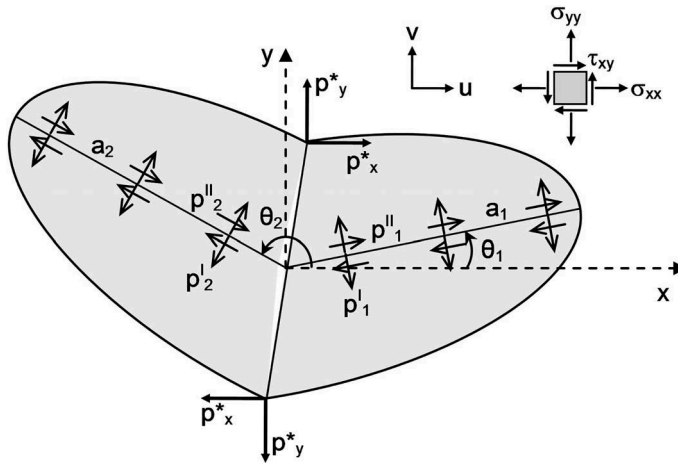
**Figure 3.** Scheme of a general kinked crack obtained as an assemblage of two elliptic semicracks (Mamani, 2015).

displacement $(u, v)$ continuity at the common points of the combined semicracks is assured. All mathematical developments including consistency and continuity checks for two elliptic semicracks are given by Dumont and Mamani (2011b). Although not developed in this paper, the demonstrations given by Dumont and Mamani (2011b) for elliptic semicracks are extensive to polynomial semicracks, as one infers by comparing the limiting cases given in Section 3.2.

In fact, the $1/\sqrt{r}$ behaviour of stresses, for $r \to 0$ at the crack tips, is observed independently from size and orientation of the semicracks. Although there is no singularity at the interface of the semicracks, a $\ln(\xi)$ term (for $\xi \to 0$) indicates that a special numerical integration scheme must be used in the vicinity of such interfaces when either $a_1 \neq a_2$ or $\theta_2 - \theta_1 \neq \pi$ (Dumont & Mamani, 2011b; Mamani, 2015).

Figure 4 schematically shows the combinations of two semicracks for the crack opening expressions given in Eqs. (16)–(19) and illustrated in Figure 3. Observe that two rotating crack shapes, when considered isolated, lead to a partial overlap of the crack faces, which is mechanically not feasible. However, this does not occur in a practical implementation as a rotation is always superposed with an opening.

In the following developments, a combination of two elliptic semicracks, as illustrated in Figure 3, will be called an *elliptic element*; the use of an elliptic semicrack and a polynomial semicrack to model the crack tip [shown as (b) in Figure 4] together with two polynomial semicracks for the crack face [shown as (a) in the figure] will be referred to as a *mixed element*; and the latter case with the additional rotating possibility, as shown in the lower row of Figure 4 for a segment either inside the crack
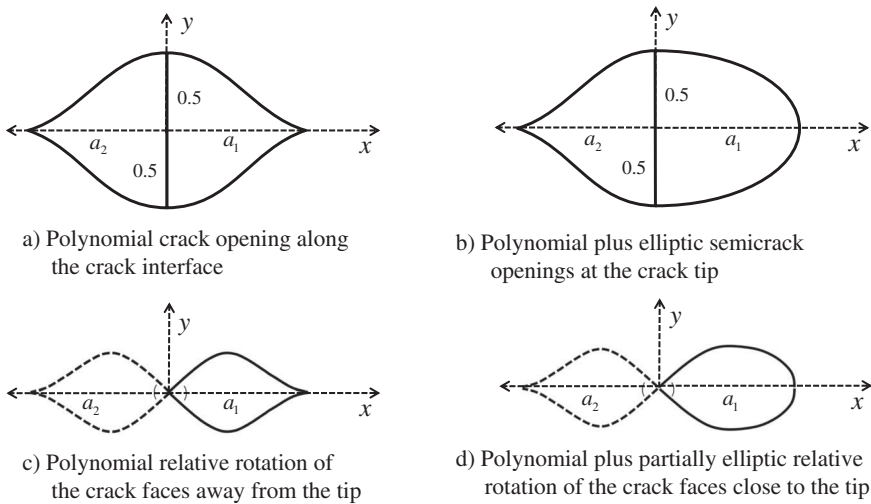
Figure 4. Combined semicrack elements used to discretise a crack in terms of openings and crack interface rotations (drilling) (Cardoso, 2017).

(c) or at the crack tip (d) will correspond to a *mixed element with rotation* and will require an additional degree of freedom to be described Mam15. The illustrations of Figures 2 and 4 can be easily visualised for a mode I crack opening, but are less intuitive in the case of Figure 3, for example, when there is a contribution of the mode II stress state. In fact, the illustrations of Figures 2 and 4 are equally valid for the mode II stress configuration, as already inferred from Eqs. (20) and (21) and comprehensively laid down by Dumont and Mamani (2011b) for the elliptic element.

## 4.2. An illustration of the combination of two semicracks

Dumont and Mamani (2011b) showed how to combine two semicracks, as described in the last section, to lead to general superpositions for elliptic and polynomial openings as well as for crack interface rotations. Although the theoretical developments by Dumont and Mamani (2011b) only address elliptic semicracks, it is in fact general as one obtains by comparing the limiting cases of $\Phi$ in Eqs. (16)–(19) and derivatives, as given in Table 1. As a matter of fact, Figure 5 illustrates a kinked crack opening due to the superposition of an elliptic and a polynomial semicracks – the relative angle between semicracks chosen to be 90° to make the three-dimensional drawing simpler. The plot was generated by sequentially using Equations (33), (62), (70), (74), (75), (78), (79), (80), (83), (84) and (85) of the mentioned paper, when generalised to also take polynomial crack openings into account. This figure is a three-dimensional representation of the scheme shown on the top right of Figure 4. One observes that the
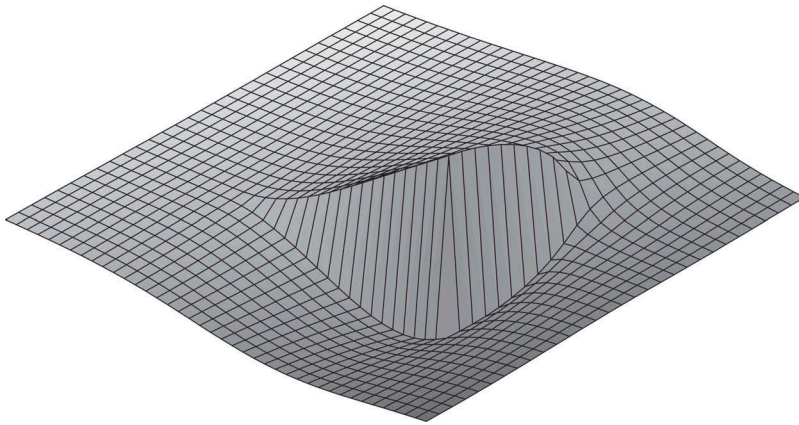
**Figure 5.** Three-dimensional illustration of a 90° kinked crack as an assemblage of a polynomial semicrack, according to Eq. (17), and an elliptic semicrack, according to Eq. (16), as schematically shown on top right of Figure 4.

cracked surface is always smooth on each side. Moreover, at most improper integrals must be dealt with and it is indeed demonstrated – see Equations (91) and (92) of that paper – that the resulting crack traction forces are always finite. However, since one is dealing with notches, in general, stress singularities may occur at points close to a notch (e.g. which is consistent with the results obtained by Williams 1957), although actually no traction force singularities occur.

### 4.3. Numerical evaluation of the crack opening

The simplest case of a horizontal crack in a continuous, isotropic and infinite medium submitted to a mode I stress field, as illustrated on the left in Figure 6, is investigated in order to numerically assess the formulation proposed in the previous section. In fact, it is the authors' experience that the numerical issues related to any complicated cracked configuration
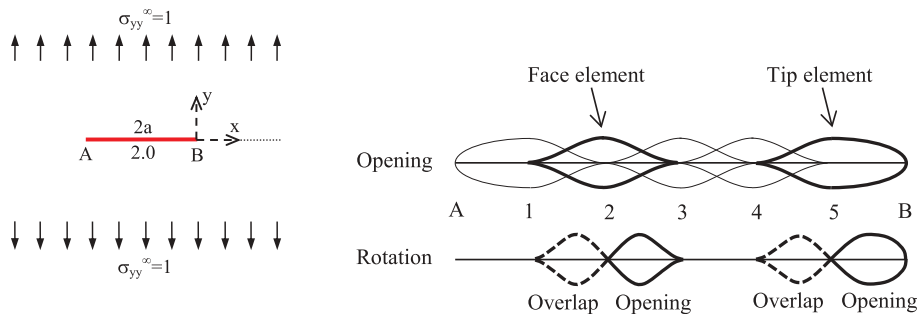


**Figure 6.** Straight crack in the open domain submitted to a remote uniaxial stress field (left), and modelling with crack elements using five nodes (right).

(including multiple and curved cracks) and any domain topology can be brought down to the stress description issues around a single, straight crack's tip (Dumont & Lopes, 2003; Dumont & Mamani, 2011b). The crack under investigation has a length $2a = 2.0$ and the material properties are such that $E/(1 - v^2) = 2$ . Thus, the target, analytical solution of this problem corresponds to an elliptic opening of unit value, as indicated on the upper left in Figure 7. The crack is modelled with combinations of elliptic and polynomial semicracks, as illustrated on the right in Figure 6 for a discretisation with five elements. All input and output quantities are given in consistent unities. When not otherwise indicated, all assessments are in terms of the HBEM.

The results for simulations with 16 nodes in terms of either elliptic elements, mixed elements or mixed elements with crack interface rotation are shown in Figure 7. Since this is a mode I problem, the former two cases actually require only one degree of freedom per element, while in the latter case there is a total of 32 degrees of freedom. The numerical results are evaluated using Eq. (7) to solve for $\mathbf{p}^*$ and then Eq. (6) to directly express the opening displacements along the crack face, as given on the upper left
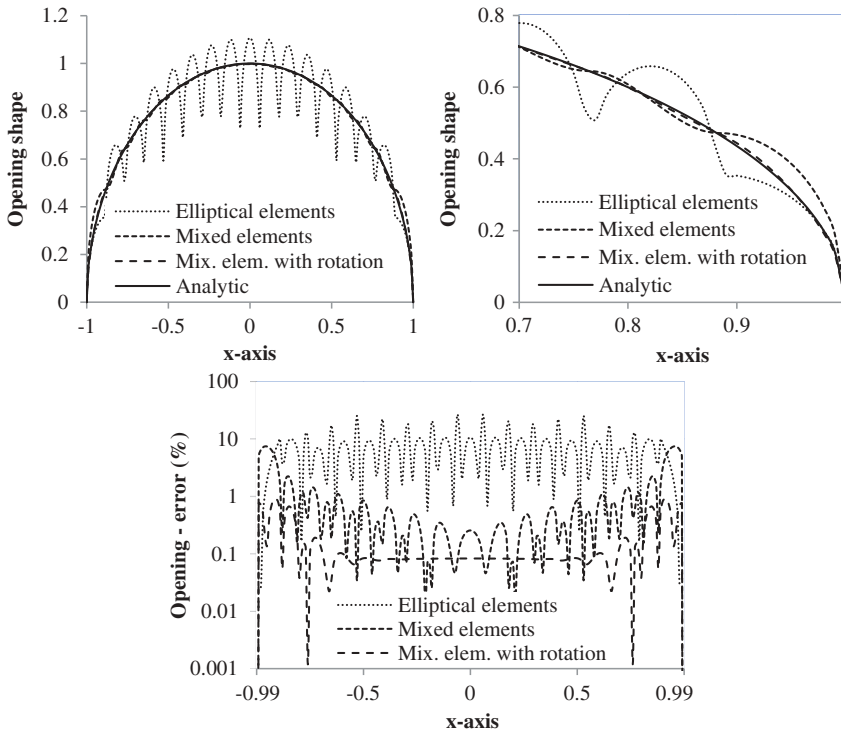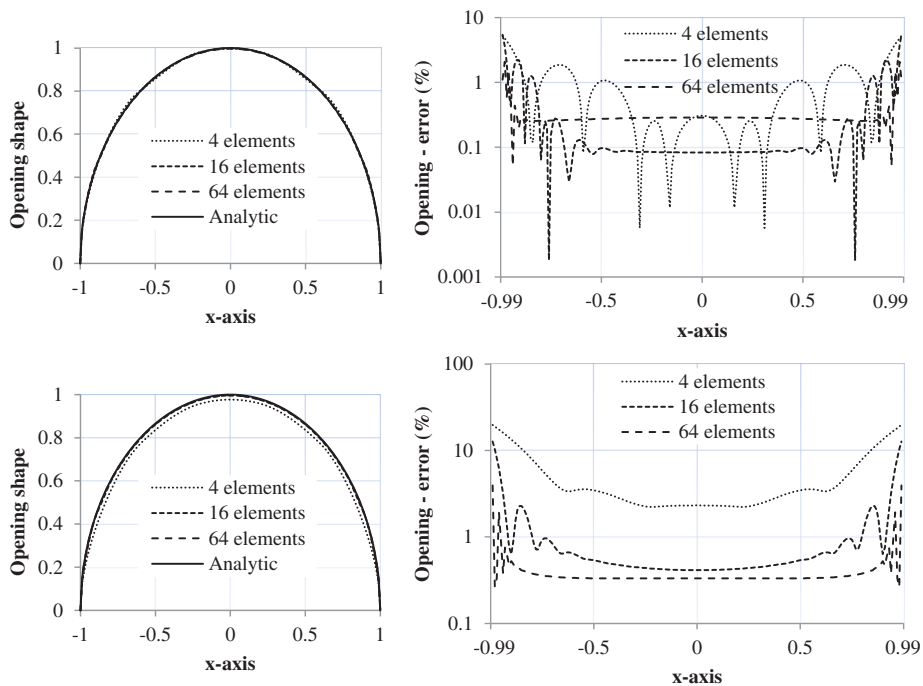


**Figure 7.** Opening displacements (upper left and zoom on the right) and corresponding errors (below) for the straight crack of Figure 6 discretised with 16 elements in an analysis with the hybrid boundary element method.

in Figure 7. The error differences can be better visualised in the bottom graph in the figure using as error norm

$$\epsilon(\%) = \left| \frac{u_{num} - u_{ana}}{u_{ana(max)}} \right| \times 100\%$$

(22)

where, in the case, $u_{ana(max)} = 1$ . The results with mixed elements are a significant improvement in comparison with the case of plain elliptic elements (both analyses with 16 degrees of freedom). The best results are by far the ones using mixed elements with rotation, although one should bear in mind that they correspond to the double amount of degrees of freedom. The graph on the upper right in Figure 7 is a zoom of the results on the left for $x \in (0.7, 1)$, to show that the added rotational degrees of freedom significantly contribute to smoothen the displacements and then arrive at more accurate results.

Figure 8 shows on the top a convergence study for the problem of Figure 6 using 4, 16 and 64 mixed elements with crack interface rotation, as implemented in the HBEM. The crack opening results are visually of excellent quality already for the case with four elements. The error analysis



**Figure 8.** Opening displacements (left) and corresponding errors (right) for the straight crack of Figure 6 using mixed elements with crack interface relative rotation in an analysis with the hybrid boundary element method (top) as well as in the conventional boundary element method (bottom).

on the right shows that the convergence is not everywhere monotonic, although this is observed globally.

### 4.3.1. *Assessment in terms of the conventional boundary element method*
The conventional boundary element method is also tested in this section. The fundamental solutions (Green's functions) proposed in Section 3 are used in the matrix system

$$\mathbf{Hd} = \mathbf{Gt} + \mathbf{b} \tag{23}$$

where $\mathbf{H}$ is the same double-layer potential matrix defined in Eq. (9), exactly as for the HBEM, and $\mathbf{G}$ is the single-layer potential matrix, which uses the same functions of Eqs. (16)–(19) to interpolate the traction forces (as implemented by Mamani 2015, although not strictly required). Since the body-force term $\mathbf{b}$ in the above equation refers to a constant stress state, it can be easily brought down to the crack boundary.

Figure 8 shows on the bottom the same kind of results of Figure 7 for opening boundary displacements interpolated from the evaluated nodal data $\mathbf{d}$ . At least in this case, the results with the conventional boundary element method are not as accurate as in the hybrid formulation (on the top). However, convergence is everywhere monotonic, as observed in the opening-error graph on the right (Cardoso,2017; Mamani, 2015).

Although the results of this section are shown in the frame of the conventional boundary element method, corresponding results for the normal stress along the crack face are given in Figure 9 as obtained using Eqs. (5) and (7) for the HBEM. On the left are the results for elliptic crack openings, and on the right are results for polynomial crack openings along the crack face.
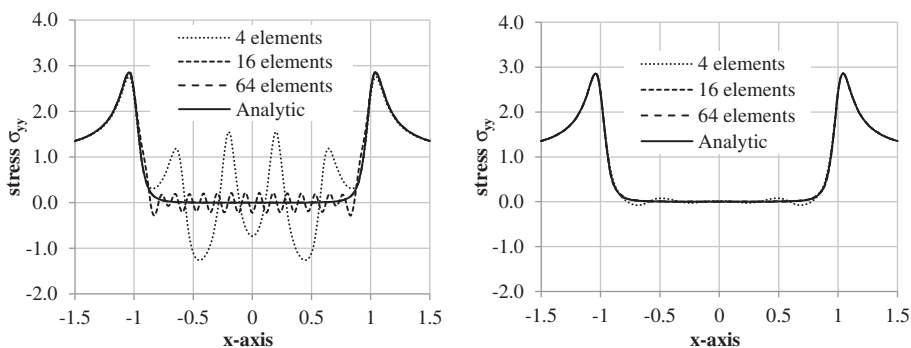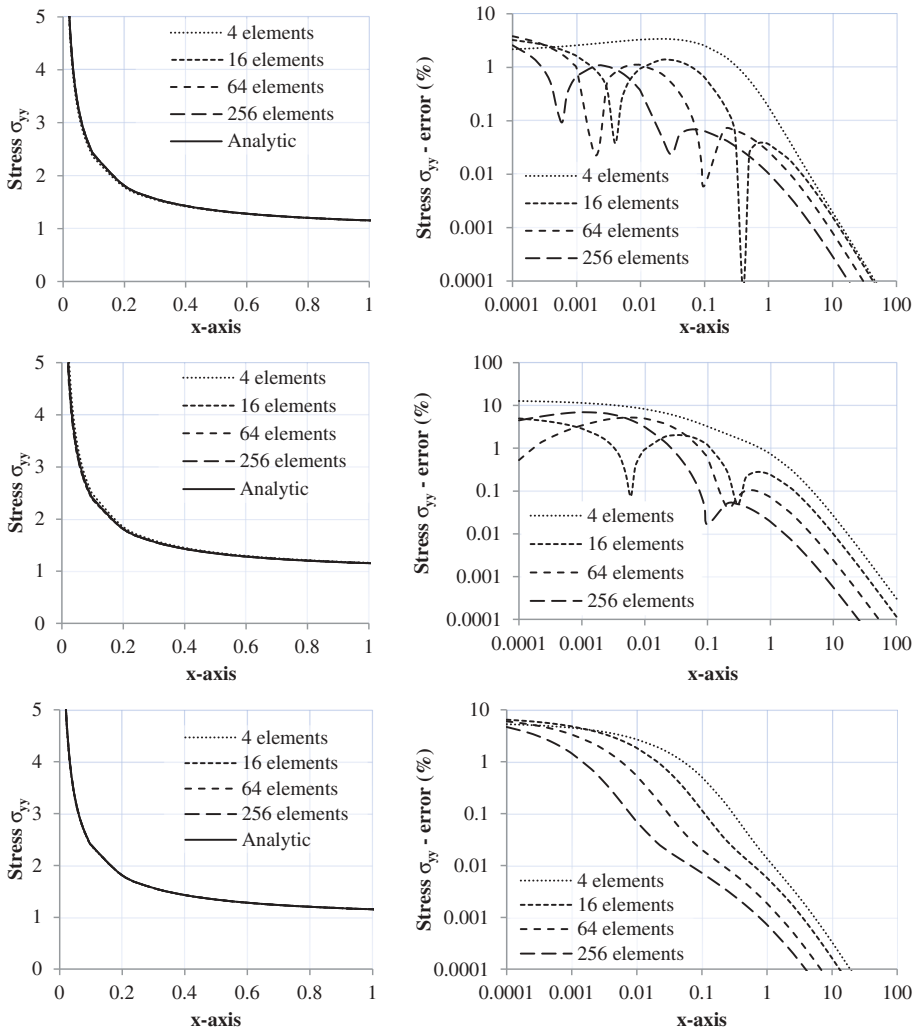


**Figure 9.** $\sigma_{yy}$ results along the crack face for elliptic semicrack elements (left) and also using mixed elements (right) in the hybrid boundary element method.

**Figure 10.** Stress $\sigma_{yy}$ values (left) and corresponding error diagrams (right) at points along the dash line on the left of Figure 6 using elliptic elements (top), mixed elements (middle) or mixed elements with crack interface rotation (bottom).

## 4.4. Assessment of the stress field around the crack tip

The same problem on the left in Figure 6 is used to assess the stress field around a crack tip. The normal stress $\sigma_{yy}$ is plotted on the top left of Figure 10 along the line segment $(x = 0..1, y = 0)$, according to the Cartesian system shown in Figure 6, for the crack modelled with different numbers of elliptic elements. The results are visually almost indistinguishable from the analytic ones. However, an analysis along the line segment $(x = 0.0001..100, y = 0)$ (top right of the figure) shows a pronounced oscillation of the errors in the near field, even though they tend to zero

for points far from the crack tip. This oscillation prevents the use of a reliable method to arrive at an accurate stress intensity factor.

The same analysis is carried out for mixed elements, as shown on the middle of Figure 10, and it is not possible to recognise an improvement in the stress field, as compared with results of the previous figure.

Finally, similar results as in the previous simulations are given on the bottom of Figure 10, but this time for simulations with mixed elements including crack interface rotation. The results improve significantly both in terms of accuracy and by presenting no oscillations as one takes into account points increasingly far from the crack tip. Then, one is entitled to conclude that this discretisation model shall lead to more robust and reliable schemes for the evaluation of stress intensity factors as well as in the estimate of the plastic zone around a crack tip.

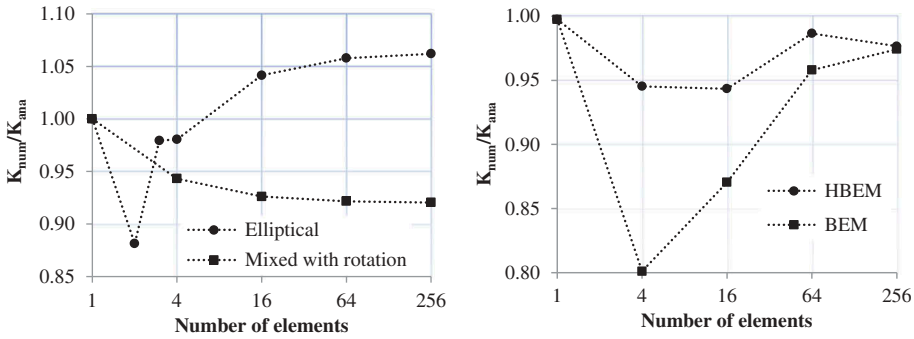### 4.5. Stress intensity factor evaluated from the force parameters $\mathbf{p}^*$

After solving Eq. (7) for the force parameters $\mathbf{p}^*$, the most immediate means of arriving at a stress intensity factor estimate is from its definition

$$K_I = \lim_{r \to 0} \sqrt{2\pi r}\sigma_{yy}(r, \theta) \tag{24}$$

for $\sigma_{yy}$ obtained from the terms of $\mathbf{p}^*$ referred to the crack tip. For the mode I problem of Figure 6 (see Mamani 2015 for the general mode I and mode II expression), one obtains

$$K_{I(n)} = \frac{\sqrt{\pi a_n}}{2a_n}\left(p^*_{y(n)} + p^*_{ry(n)}\right) \tag{25}$$

where $a_n$ is the semicrack length at the crack tip (it would be $a_1$ on the right in Figure 4) and $p^*_{y(n)}$ and $p^*_{ry(n)}$ are the force parameters corresponding to the opening shapes – relative displacement and crack interface rotation – on the right of the same Figure 4. The results for 1, 4, 16, 64 and 256 elements are given on the left in Figure 11. Although the results have been shown to converge for stresses in the vicinity of the crack tip, as in the previous figures, absolute convergence cannot be observed in this case – and cannot be demonstrated by any theorem, since this is a localised behaviour (how the stress goes locally to infinity) for which no energy norm can be given (Dumont & Lopes, 2003). It is even surprising that the results for elliptic elements do converge better than in the case of the generally more accurate implementation with mixed elements with crack interface rotation (6% accuracy against 8%). Also, observe that, in the present case, the result for just one crack element trivially coincides with the analytic solution.

**Figure 11.** Stress intensity factors for the straight crack of Figure 6 obtained (left) from Eq. (25) for elliptic and mixed elements with rotation and (right) in terms of the crack tip opening displacement.

### 4.6. Stress intensity factor evaluated from the crack tip opening

The stress intensity factor may be obtained from the crack tip opening displacement:

$$K_I = \frac{2G}{\kappa + 1} \lim_{r \to 0} \sqrt{\frac{2\pi}{r}} u_y(r, \pi) \tag{26}$$

where $\kappa = 3 - 4v$ for plane strain and $\kappa = (3 - v)/(1 + v)$ for plane stress. Such results are usually more accurate than in terms of the stress field, as shown on the right in Figure 11 for $u_y$ evaluated at a distance of 0.01 from the crack tip using the hybrid as well as the conventional boundary element methods. Although no convergence can be demonstrated also in this case, the results (errors $\approx$ 3%) are better than the ones reported by Anderson (1995) for a finite element mesh with 2000 nodes (errors $\approx$ 5%).

### 4.7. Stress intensity factor evaluated from stresses

For the crack of Figure 6, a simple and direct estimate of the stress intensity factor is by using Eq. (24), where in practice $r$ is given a very small value, also with $\theta = 0$. The analytical solution for the crack problem of Figure 6 is $K_I = \sqrt{\pi}$. The graph on the left in Figure 12 shows the relation between numerically evaluated stress intensity factors for $r = 0.001, 0.01$ and $0.1$, using Eq. (24), and the analytical, target one. Another possibility would be the extrapolation of the above values to obtain results at $r = 0$. However, there is an oscillation as $r \to 0$, which renders such a procedure not reliable.

An alternative to estimate the stress intensity factor is by comparison with the Williams' series, as explored, for instance, by Lopes (2002). As
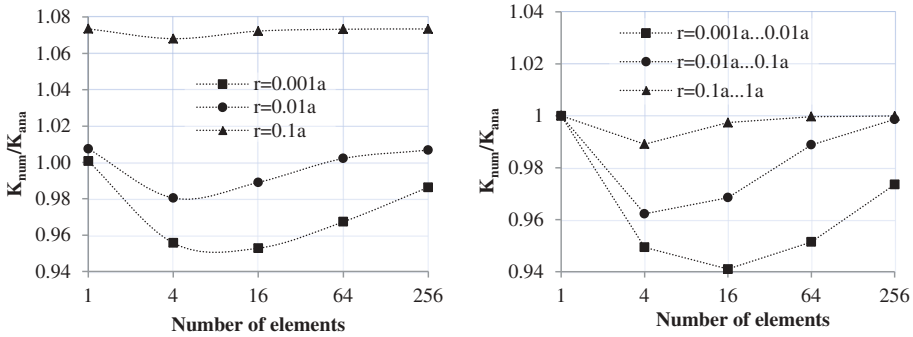
**Figure 12.** Stress intensity factors of the straight crack of the Figure 6 obtained at several close points $r$ (left) as well as in terms of the Williams' series (right).

first shown by Williams (1957), the stress expression around a crack tip is, in polar coordinates,

$$\sigma_{rr} = \frac{1}{4\sqrt{r}} \left[ s_1 \left( -5\cos\frac{\theta}{2} + \cos\frac{3\theta}{2} \right) + t_1 \left( -5\sin\frac{\theta}{2} + 3\sin\frac{3\theta}{2} \right) \right] + 4s_2\cos^2\theta...$$

(27)

$$\sigma_{\theta\theta} = \frac{1}{4\sqrt{r}} \left[ s_1 \left( -3\cos\frac{\theta}{2} - \cos\frac{3\theta}{2} \right) + t_1 \left( -3\sin\frac{\theta}{2} - 3\sin\frac{3\theta}{2} \right) \right] + 4s_2\sin^2\theta...$$

(28)

$$\sigma_{r\theta} = \frac{1}{4\sqrt{r}} \left[ s_1 \left( -\sin\frac{\theta}{2} - \sin\frac{3\theta}{2} \right) + t_1 \left( \cos\frac{\theta}{2} + 3\cos\frac{3\theta}{2} \right) \right] - 2s_2\sin2\theta...$$

(29)

The constants $s_1$ and $t_1$ are related to mode I and mode II stress intensity factors by

$$s_1 = -\frac{K_I}{\sqrt{2\pi}} \quad and \quad t_1 = \frac{K_{II}}{\sqrt{2\pi}}$$

(30)

Then, it is possible to evaluate $\sigma_{yy}$ at a series of points departing from as close as possible to $r = 0$ along the $x$ axis and fit using least squares the series given according to Eqs. (27)–(29).

The graph on the right in Figure 12 displays the stress intensity factor results for five terms of the Williams' series (the first term is the one of actual interest) obtained from 10 numerical values $\sigma_{yy}$ for $r \in (0.001, 0.01)$, $r \in (0.01, 0.1)$ and $r \in (0.01, 0.1)$ along the $x$ axis. Observe that the analytic solution is trivially obtained for one single crack element.

## 5. Concluding remarks

The implemented crack tip elements provide a simple and efficient means for the description of the stress field around crack tips. Although the combination of generalised Westergaard functions and Kelvin's fundamental solutions has shown to be efficient in terms of the global behaviour of a cracked elastic body (Dumont & Lopes, 2003; Dumont & Mamani, 2011b, 2013; Lopes, 1998, 2002; Mamani, 2011, 2015), some improvements have become mandatory from the preliminary investigations as regarding the very local phenomenon of stresses going to infinity. In fact, the elliptic semicracks, which seem efficient for the description of the stress field around crack tips, must be combined with crack elements of different shapes, so that spurious high stress gradients along the crack face can be avoided or minimised, as shown by means of several numerical assessments. The numerical examples of Section 4 have been analysed for biaxial stress states, as well, with similar results as the ones displayed. The present developments for a single straight crack in the open domain lead to a better understanding of the more complex cases of multiply connected and multiply cracked, irregularly shaped domains under complicated load combinations. Evaluations of the stress intensity factor in terms of the J integral have already been carried out by Lopes (2002) and Mamani (2011, 2015) using only elliptic elements. Evaluations for the J integral using the proposed improved elements, not given in this paper, show improvements, which are however not significant. The general conclusion is that no monotonic convergence can be demonstrated for evaluations of stress intensity factors since there seems to be no energy theorem related to this local phenomenon. A code for general applications is available and some results have already been published (Dumont & Lopes, 2003; Dumont & Mamani, 2011b). The code for the simulation of plastic zones around crack tips, as developed by Dumont and Mamani (2013), is now being implemented with the more general shapes proposed in this paper. Although all theoretical and computational developments for the two-dimensional analysis of fracture mechanics have already been carried out in the present framework, one is still missing a general purpose code that combines all kinds of fundamental solutions as Kelvin's fundamental solution cannot be matched when the aim is to represent far field effects (Lopes, 2002; Mamani, 2015). One interesting investigation would be the comparison of stress results coming from the Somigliana's identity with the direct results obtained according to this paper. Such evaluation of high stress gradients arbitrarily close to nodal points using Somigliana's identity has been made possible by the numerical evaluation procedure proposed by Dumont (1994, 2018)).

## Disclosure statement

## Funding

## ORCID

Ney Augusto Dumont   http://orcid.org/0000-0003-4147-3130
Elvis Yuri Mamani   http://orcid.org/0000-0001-6139-0960
Marilene Lobato Cardoso   http://orcid.org/0000-0002-2206-0157

## References

Anderson, T. L. (1995). *Fracture mechanics: Fundamentals and applications*. 2$^{nd}$ edition. C. R. C. Press. Boca Raton, New York

Ang, W. T., & Telles, J. C. F. (2004). A numerical Green's function for multiple cracks in anisotropic bodies. *Journal of Engineering Mathematics*, *49*(3), 197–207.

Barenblatt, G. I. (1962).The mathematical theory of equilibrium cracks in brittle fracture. In *Advances in applied mechanics*. VII, 55–129. Academic Press: Amsterdam.

Brebbia, C. A., Telles, J. C. F., & Wrobel, L. C. (1984). *Boundary element techniques: Theory and applications in engineering*. Berlin: Prentice Hall.

Brown, W. F., & Strawley, J. E. (1966). Plane strain crack toughness testing of high strength metallic materials. In *ASTM STP 410* (pp. 5). American Society For Testing And Materials: Philadelphia, PA.

Cardoso, M. L. (2017). *A boundary element implementation for fracture mechanics problems using generalized westergaard stress functions*. MSc. thesis (in Portuguese), Pontifical Catholic University of Rio de Janeiro, Brazil.

Crouch, S. L., & Starfield, A. M. (1983). *Boundary element methods in solid mechanics*. London: George Allen & Unwin.

Dugdale, D. S. (1960). Yielding in steel sheets containing slits. *Journal of the Mechanics and Physics of Solids*, *8*, 100–104.

Dumont, N. A. (1989). The hybrid boundary element method: An alliance between mechanical consistency and simplicity. *Applied Mechanics Reviews*, *42*(11–2), S54–S63.

Dumont, N. A. (1994). On the efficient numerical evaluation of integrals with complex singularity poles. *Engineering Analysis with Boundary Elements*, *13*, 155–168.

Dumont, N. A. (2014). The hypersingular boundary element method revisited. In C. A. Brebbia & A. H.-D. Cheng (eds), *Boundary elements and other mesh reduction methods XXXVII, WIT transactions on modelling and simulation* (Vol. 57, pp. 27–39).

Dumont, N. A. (2018). The collocation boundary element method revisited: Perfect code for 2D poblems. *International Journal Comparative Meth and Experiments Measurement*, *6*(6), 965–975.

Dumont, N. A., & Aguilar, C. A. (2012). The best of two worlds: The expedite boundary element method. *Engineering Structures*, *43*, 235–244.

Dumont, N. A., Chaves, R. P., & Paulino, G. H. (2004). The hybrid boundary element method applied to problems of potential of functionally graded materials. *International Journal of Computational Engineering Science (IJCES)*, 5(4), 863–891.

Dumont, N. A., & De Oliveira, R. (2001). From frequency-dependent mass and stiffness matrices to the dynamic response of elastic systems. *International Journal of Solids and Structures*, 38(10–13), 1813–1830.

Dumont, N. A., & Huaman, D. (2009). Hybrid finite/boundary element formulation for strain gradient elasticity problems. In E. J. Sapountzakis & M. H. Aliabadi, eds., *Advances in Boundary Element Techniques* X, *Proceedings of the 10th International Conference*, pp. 295–300, EC, Ltd., UK.

Dumont, N. A., & Lopes, A. A. O. (2003). On the explicit evaluation of stress intensity factors in the hybrid boundary element method. *Fatigue & Fracture of Engineering Materials & Structures*, 26, 151–165.

Dumont, N. A., & Mamani, E. Y. (2011a). Use of generalized Westergaard stress functions as fundamental solutions. In E. L. Albuquerque & M. H. Aliabadi (eds), *Advances in boundary element techniques XII* (pp. 170–175). UK: EC, Ltd.

Dumont, N. A., & Mamani, E. Y. (2011b). Generalized Westergaard stress functions as fundamental solutions. *Computer Modeling in Engineering & Sciences*, 78(2), 109–150.

Dumont, N. A., & Mamani, E. Y. (2013). Simulation of plastic zone propagation around crack tips using the hybrid boundary element method. In Z. J. G. N. Del Prado ed, *CILAMCE – XXXIV iberian latin-american congress on computational methods in engineering* 20 pp on CD. Pirenópolis, Brazil

Dumont, N. A., Mamani, E. Y., & Cardoso, M. L. (2017). A boundary element implementation for fracture mechanics problems using generalized Westergaard stress functions. In L. Marin & M. H. Aliabadi (eds), *Advances in boundary element & meshless techniques XVIII* (pp. 120–125). UK: LC, Ltd.

Eftis, J., & Liebowitz, H. (1972). On the modified Westergaard equations for certain plane crack problems. *International Journal of Fracture Mechanics*, 8(4), 383–392.

Gupta, M., Alderliesten, R. C., & Benedictus, R. (2015). A review of T-stress and its effects in fracture mechanics. *Engineering Fracture Mechanics*, 134, 218–241.

Harmain, G. A., & Provan, J. W. (1997). Fatigue crack-tip plasticity revisited – The issue of shape addressed. *Theory and Application Fracture Mechanics*, 26, 63–79.

Irwin, G. R. (1957). Analysis of stresses and strain near the end of a crack traversing a plate. *Journal of Applied Mechanics*, 24, 361–364.

Jing, P., Khraishi, T., & Gorbatikh, L. (2003). Closed-form solutions for the mode II crack tip plastic zone shape. *International Journal of Fracture*, 122, 137–142.

Lopes, A. A. O. (1998). *The hybrid boundary element method applied to fracture mechanics problems*. MSc. thesis (in Portuguese), Pontifical Catholic University of Rio de Janeiro, Brazil.

Lopes, A. A. O. (2002). *Evaluation of stress intensity factors with the hybrid boundary element method*. PhD. thesis (in Portuguese), Pontifical Catholic University of Rio de Janeiro, Brazil.

Mamani, E. Y. (2011). *The hybrid boundary element method based on generalized Westergaard stress functions*. MSc. thesis (in Portuguese), Pontifical Catholic University of Rio de Janeiro, Brazil.

Mamani, E. Y. (2015). *Crack modeling using generalized Westergaard stress functions in the hybrid boundary element method*. PhD. thesis (in Portuguese), Pontifical Catholic University of Rio de Janeiro, Brazil.

Mamani, E. Y., & Dumont, N. A. (2015). Use of improved Westergaard stress functions to adequately simulate the stress field around crack tips. In N. A. Dumont ed, *CILAMCE –*

*XXXVI iberian latin-american congress on computational methods in engineering* (17). ISSN: 2178-4949. doi:10.20906/CPS/CILAMCE2015-0840http://www.swge.inf.br/proceedings/CILAMCE2015/ Rio de Janeiro, Brazil

Pian, T. H. H. (1964). Derivation of element stiffness matrices by assumed stress distribution. *AIAA Journal*, *2*, 1333–1336.

Sneddon, I. N. (1946). The distribution of stress in the neighborhood of a crack in an elastic solid. *Proceedings of the Royal Society of London A*, *187*, 229–260.

Sousa, R. A., Castro, J. T. P., Lopes, A. A. O., & Martha, L. F. (2013). On improved crack tip plastic zone estimates based on t-stress and on complete stress fields. *Fatigue & Fracture of Engineering Materials & Structures*, *36*(1), 25–38.

Tada, H., Ernst, H., & Paris, P. (1993). Westergaard stress functions for displacement-prescribed crack problems - I. *International Journal of Fracture*, *61*, 39–53.

Tada, H., Ernst, H., & Paris, P. (1994). Westergaard stress functions for displacement-prescribed crack problems - II. *International Journal of Fracture*, *67*, 151–167.

Telles, J. C. F., Castor, G. S., & Guimares, S. (1995). A numerical Green's function approach for boundary elements applied to fracture mechanics. *International Journal for Numerical Methods in Engineering*, *38*, 3259–3274.

Westergaard, H. M. (1939). Bearing pressures and cracks. *Journal of Applied Mechanics*, *6*, 49–53.

Williams, M. L. (1957). On the stress distribution at the base of a stationary crack. *Journal of Applied Mechanics*, *24*, 109–114.

Xin, G., Hangong, W., Xingwu, K., & Liangzhou, J. (2010). Analytic solutions to crack tip plastic zone under various loading conditions. *European Journal of Mechanics A/Solids*, *29*, 738–745.

Zhang, Y., Qiang, H., & Yang, Y. (2007). Unified solutions to mixed mode crack tip under small scale yielding. *Chinese Journal of Mechanical Engineering*, *43*(2), 50–54.